QCD corrections to $t\bar{t}b\bar{b}$ productions via photon-photon collisions at linear colliders

Guo Lei, Ma Wen-Gan, Han Liang, Zhang Ren-You, and Jiang Yi
Department of Modern Physics, University of Science and Technology
of China (USTC), Hefei, Anhui 230027, P.R.China

Abstract

We calculated the complete next-to-leading order(NLO) QCD corrections to the $t\bar{t}b\bar{b}$ production process at a $\gamma\gamma$ collider in the standard model(SM). The calculation of the one-loop QCD correction includes the evaluations of the hexagon and pentagon amplitudes. We studied the NLO QCD corrected total cross section, the distributions of transverse momenta of final top- and bottom-quark states, and the dependence of the cross section on renormalization scale μ. It shows that NLO QCD correction generally increases the LO cross section in our chosen parameter space, and the K-factor varies from 1.70 to 1.14 when colliding energy goes up from 400 GeV to 2 TeV. We find that the correction distinctly changes the distributions of transverse momenta of the final top- and bottom-quark states, and the NLO QCD correction obviously improves the independence of the cross section for process $\gamma\gamma \to t\bar{t}b\bar{b}$ on the renormalization scale.

PACS: 14.65.Ha, 14.80.Bn, 12.38.Bx

I. Introduction

Recently, the report of the top-quark mass measurements from the CDF and D0 experiments at Fermilab, presents the preliminary world average mass of the top quark is $m_t = 172.5 \pm 1.3(stat) \pm 1.9(syst)\ GeV$, which corresponds to a 20% precision improvement relative to the previous combination[1]. Due to the huge top-quark mass being much heavier than the W-boson, before the top-quark hadronization it undergoes dominantly the weak decay via $t \to W^+b$[2], that has two important consequences different with other quarks, the narrow resonance around the energy $2m_t$ is absent and the perturbative QCD is reliable to study all the threshold region. We believe the large top mass value will open up new vistas of electroweak physics and possibilities for probing the effects beyond the SM. For example, since the Higgs mechanism in the SM and other extended models predicts that the strength of quark-Higgs Yukawa coupling is proportional to the quark mass[3], one can measure top-quark Yukawa couplings in high precision to probe the SM or discover new physics. There have been many works concerning the study of the top-quark physics at colliders [4, 5, 6, 7, 8]. All those indicate that the precise study of the top physics is accessible. In the proposed and planned experiments, such as at the CERN LHC and the ILC, more interests are focused on the developing and understanding top physics and top characteristics.

The future e^+e^- linear collider(LC) not only can be designed to operate in e^+e^- collision mode, but also can be operated as a $\gamma\gamma$ collider. This is achieved by using Compton backscattered photons in the scattering of intense laser photons on the initial e^+e^- beams. The top-quark pair production at photon-photon collider is also useful for top-quark physics study. It has been found that the $\gamma\gamma \to t\bar{t}$ production rate with high $\gamma\gamma$ colliding energy, is much larger than that from the direct $e^+e^- \to t\bar{t}$ production due to the s-channel suppression of later process [9, 10, 11].

At the future International e^+e^- Linear Collider (ILC), the colliding center-of-mass-system (c.m.s.) energy can be raised up to 2 TeV. At TeV scale high colliding energy, the final states will be very complex and expected to be in multi-particles or jets with large production rates, and top and Higgs signatures naturally are included in these processes. For these processes with large cross sections, a leading order analysis is not adequate to make detailed predictions for their

cross sections. In fact, the processes with multiple final particles are particularly interesting, since such processes often proceed through one or more resonances that subsequently decay, or they represent an irreducible background to such resonance processes. For example, the associated production $\gamma\gamma \to t\bar{t}H$ is an important process in probing top-Higgs Yukawa coupling in high precision, and was already studied in Ref.[12]. But after Higgs boson and top-quark decay, the $t\bar{t}H$ associated production process at $\gamma\gamma$ collider would have the same final states ($W^+bW^-\bar{b}b\bar{b}$) as the process $\gamma\gamma \to t\bar{t}b\bar{b}$. Therefore, it is important to emphasize that the ability to distinguish top, Higgs boson or other new particle signatures at linear colliders, crucially depends on the understanding of the corresponding backgrounds of the corresponding processes with multi-particle final states. In order to exert all the abilities of future colliders, precise theoretical predictions including higher order corrections to multi-particle production processes are necessary.

In previous work, people used "double-pole approximation" (DPA) [13] to handle the evaluations of complete one-loop strong and electroweak calculation for process including four particle final states. Recently, the methods for the calculation of scalar and the tensor 6-point integral functions were provided[14, 16]. With the approach provided in Ref.[14], the complete electroweak corrections to the $e^+e^- \to 4f$ processes, which are relevant for W-pair production, was presented by A. Denner, S. Dittmaier, M. Roth, L.H. Wieders, and the results were compared with those in Ref.[17] by using DPA method.

In this paper we present the calculations of the cross sections of the process $\gamma\gamma \to t\bar{t}b\bar{b}$ at the leading-order(LO) ($\mathcal{O}(\alpha_{ew}^2\alpha_s^2)$) and QCD next-to-leading-order(NLO) ($\mathcal{O}(\alpha_{ew}^2\alpha_s^3)$). The paper is organized as follow: The tree-level analytical calculation of the cross section for the process $\gamma\gamma \to t\bar{t}b\bar{b}$ is given in section II. In section III the analytical calculation of the NLO QCD corrections is presented. The numerical results and discussions are given in section IV. Finally, a short summary is given in section V.

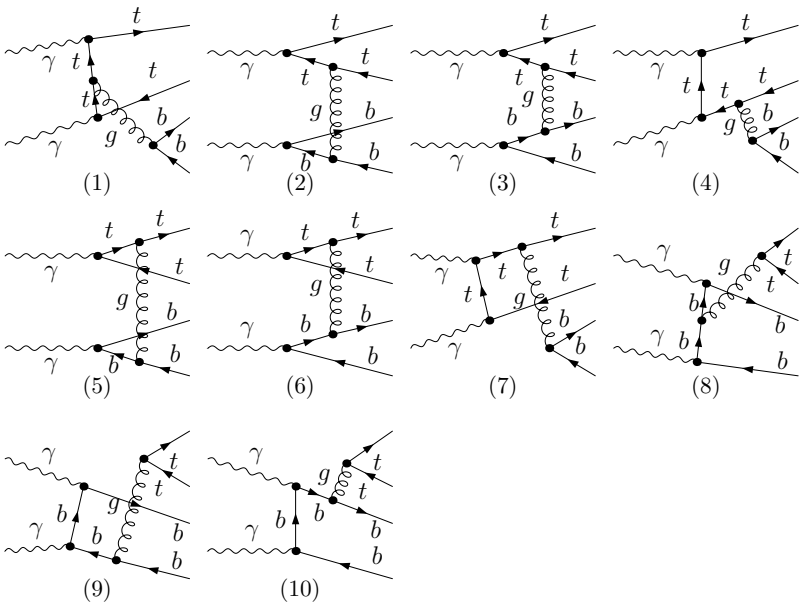

Figure 1: The t-channel tree-level Feynman diagrams at the $\mathcal{O}(\alpha_{ew}\alpha_s)$ order for $\gamma\gamma \to t\bar{t}b\bar{b}$.

II. Analytical calculation of the cross section for the process $\gamma\gamma \to t\bar{t}b\bar{b}$ at the tree-level($\mathcal{O}(\alpha_{ew}^2\alpha_s^2)$)

The process $\gamma\gamma \to t\bar{t}b\bar{b}$ can be induced via $t-$ and $u-$channel at the tree-level. In this section we consider the tree-level($\mathcal{O}(\alpha_{ew}^2\alpha_s^2)$) contribution to the cross section for the process $\gamma\gamma \to t\bar{t}b\bar{b}$. We denote the process as

$$\gamma(p_1) + \gamma(p_2) \to t(p_3) + \bar{t}(p_4) + b(p_5) + \bar{b}(p_6), \tag{2.1}$$

where the four-momenta of incoming photons are denoted as p_1 and p_2, and p_3, p_4, p_5, p_6 represent the four-momenta of the final particles. The FeynArts3.2 package[18] is adopted to generate tree-level Feynman diagrams and convert them to corresponding amplitudes. We present the t-channel tree-level Feynman diagrams involving strong interaction for the process $\gamma\gamma \to t\bar{t}b\bar{b}$ in Fig.1. The u-channel diagrams, which can be obtained by exchanging initial photons of the corresponding t-channel ones, are not drawn there.

The tree-level amplitude $\mathcal{M}$ of the process $\gamma\gamma \to t\bar{t}b\bar{b}$ at the $\mathcal{O}(\alpha_{ew}\alpha_s)$ order, is then expressed as below.

$$\mathcal{M} = \sum_{i=1}^{10} \sum_{j=u}^{t} \mathcal{M}_j^{(i)}. \tag{2.2}$$

where the amplitudes ($\mathcal{M}_t^{(i)},\ i = 1, ..., 10$) correspond to the diagrams in Fig.1(1-10) respectively.

Then we get the differential cross section for the process $\gamma\gamma \to t\bar{t}b\bar{b}$ at the tree-level as

$$d\sigma_{tree} = \overline{\sum} |\mathcal{M}|^2 \, d\Phi_4, \tag{2.3}$$

where $d\Phi_4$ is the four-body phase space element. The summation is taken over the spins and colors of final states, and the bar over the summation in Eq.(2.3) recalls averaging over initial spin states. The calculation of the amplitudes of tree-level diagrams for $\gamma\gamma \to t\bar{t}b\bar{b}$ process is implemented by using FormCalc4.1 package[19]. The integration program of the four-body phase space is based on the FormCalc4.1 package, and created by using the factorization expression of four-body phase space element[20],

$$d\Phi_4(p_1+p_2, p_3, p_4, p_5, p_6) = \frac{1}{2\pi} dQ^2 d\Phi_3(p_1+p_2, p_3, p_4, Q) d\Phi_2(Q, p_5, p_6). \tag{2.4}$$

where $Q \equiv p_5 + p_6$ and the actual integration of three-body phase space element $d\Phi_3(p_1 + p_2, p_3, p_4, Q)$ is parameterized using 2to3.F program in FormCalc4.1 package[19], and the complete integration over the four-body phase space is performed using Monte Carlo integrator Vegas. The two-body phase space $d\Phi_2(Q, p_5, p_6)$ is given as

$$d\Phi_2(Q, p_5, p_6) = \frac{1}{(2\pi)^2} \frac{\sqrt{\lambda(Q^2, m_5^2, m_6^2)}}{8Q^2} d\varphi_5 d(cos\theta_5), \tag{2.5}$$

where the kinematical function $\lambda(x, y, z)$ is defined by

$$\lambda(x, y, z) = x^2 + y^2 + z^2 - 2xy - 2yz - 2zx. \tag{2.6}$$

In order to check our four-body phase space integration program, we calculated the LO cross section of $e^+e^- \to u\bar{d}\mu^-\bar{\nu}_\mu$ process by adopting fixed-width method and the same input parameters as used in Ref.[17]. In Table 1 we list the the LO cross sections obtained from Ref.[17], by using GRACE2.2.0 system[21], and by adopting our 4-body phase space integration program together with FeynArts3.2 and FormCalc4.1, respectively. It demonstrates the numerical integration results by using our created program are in good agreement with others.

III. The NLO QCD corrections to the process $\gamma\gamma \to t\bar{t}b\bar{b}$

The FeynArts3.2 package is used to generate QCD one-loop Feynman diagrams of $\gamma\gamma \to t\bar{t}b\bar{b}$ process at the order of $\mathcal{O}(\alpha_{ew}\alpha_s^2)$, and then to convert them to corresponding amplitudes. The

$\sqrt{s}(GeV)$	$\sigma_{LO}(fb)$(Ref.[17])	$\sigma_{LO}(fb)$(GRACE)	$\sigma_{LO}(fb)$(ours)
200	661.3(3)	661.24(3)	661.26(4)
500	260.9(1)	260.85(2)	260.87(2)

Table 1: The comparison of the numerical results of the LO cross section for $e^+e^- \to u\bar{d}\mu^-\bar{\nu}_\mu$ process by using GRACE2.2.0 system and our integration program with those presented in Ref.[17].

QCD one-loop Feynman diagrams can be classified into 140 self-energy diagrams, 172 triangle diagrams, 108 box diagrams, 48 pentagon diagrams and 12 hexagon diagrams. We also use the FormCalc4.1 package[19] to calculate the amplitudes of one-loop Feynman diagrams. But the original FormCalc4.1 package doesn't possess the function to calculate the amplitudes including 6-point integrals, we have to create some codes in FormCalc4.1 in order to handle amplitudes relevant to hexagon diagrams. As a representative selection, we present the hexagon Feynman diagrams of the $\gamma\gamma \to t\bar{t}b\bar{b}$ process in Fig.2. There exist both ultraviolet(UV) divergency and soft infrared(IR) singularity in the contribution part of virtual gluon one-loop diagrams for $\gamma\gamma \to t\bar{t}b\bar{b}$ process, but no collinear IR singularity due to the nonzero masses of top and bottom quark. Dimensional regularization(DR) scheme in $D = 4 - 2\epsilon$ dimensions is adopted to isolate both IR and UV singularities. By adopting $\overline{MS}$-scheme to renormalize the strong coupling strength and the OS-scheme to renormalize the masses and fields of top- and bottom-quark, the UV singularities are vanished.

In the total cross section, the soft IR divergency contributed by the virtual correction part should be cancelled by the contribution from real gluon emission process $\gamma\gamma \to t\bar{t}b\bar{b} + g$ at tree-level($\mathcal{O}(\alpha_{ew}^2\alpha_s^3)$), which presents the same order contribution as the virtual correction does. The real gluon emission process is denoted as

$$\gamma(p_1) + \gamma(p_2) \to t(p_3) + \bar{t}(p_4) + b(p_5) + \bar{b}(p_6) + g(p_7). \tag{3.1}$$

We adopt the two cutoff phase-space slicing(TCPSS) method[22] to calculate the real gluon emission process. Since there is no collinear IR singularity, we introduce only an arbitrary small soft cutoff δ_s to separate the $\gamma\gamma \to t\bar{t}b\bar{b} + g$ phase space into two regions, according to whether the energy of the emitted gluon is soft($E_7 \leq \delta_s\sqrt{s}/2$) or hard($E_7 > \delta_s\sqrt{s}/2$). After a lengthy calculation similar with those shown in references [23, 24, 25, 26], we can get the expression of

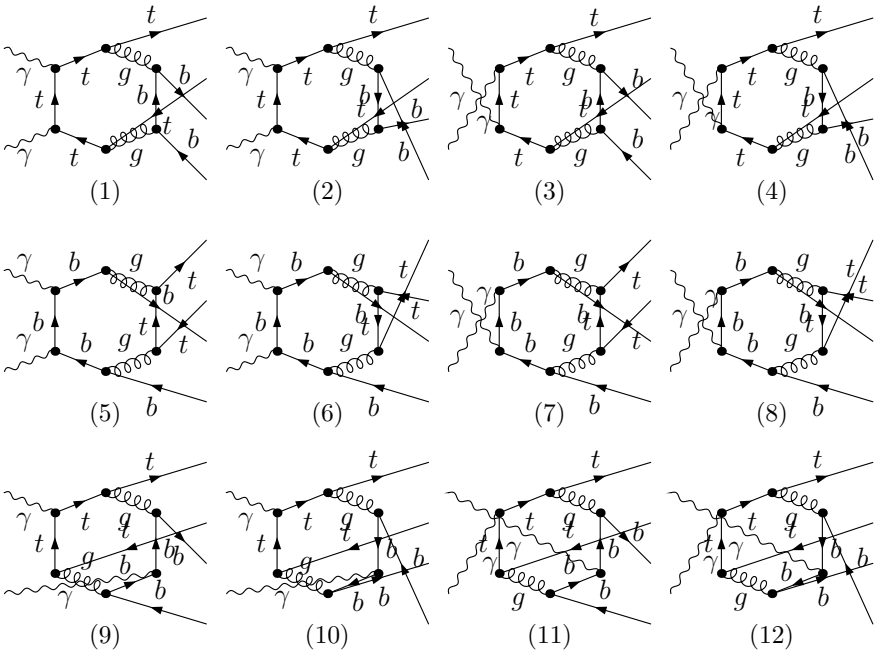

Figure 2: The hexagon Feynman diagrams for $\gamma\gamma \to t\bar{t}b\bar{b}$ process.

σ_{soft} for $\gamma\gamma \to t\bar{t}b\bar{b}$ process as,

$$\sigma_{soft} = \frac{\alpha_s}{2\pi}\left[\frac{1}{3}\left(g_{35}+g_{46}\right)+\frac{7}{6}\left(g_{36}+g_{45}\right)-\frac{1}{6}\left(g_{34}+g_{56}\right)\right]\sigma_{tree}, \tag{3.2}$$

where g_{ij} $(i,j=3,4,5,6)$ are defined as,

$$\begin{aligned} g_{ij}(p_i,p_j) &= \left(\frac{\pi\mu^2}{\Delta E^2}\right)^{\epsilon}\Gamma(1+\epsilon)\left[\frac{2(p_ip_j)}{\lambda^{1/2}(s_{ij},m_i^2,m_j^2)}\ln(\sigma_i\sigma_j)+2\right]\frac{1}{\epsilon}-\frac{2(p_ip_j)}{\lambda^{1/2}(s_{ij},m_i^2,m_j^2)} \\ &\quad\times\left[\frac{1}{2}\ln^2(\sigma_i)+\frac{1}{2}\ln^2(\sigma_j)+2Li_2\left(1-\sigma_i\right)+2Li_2\left(1-\sigma_j\right)\right] \\ &\quad-\frac{1}{\rho_i}\ln\sigma_i-\frac{1}{\rho_j}\ln\sigma_j+\mathcal{O}(\epsilon), \qquad (i,j=3,4,5,6,\ i<j). \end{aligned} \tag{3.3}$$

In above equation, $\lambda(s_{ij},m_i^2,m_j^2)$ is the kinematical function defined in Eq.(2.6), $\Delta E=\delta_s\sqrt{s}/2$, $s_{ij}=(p_i+p_j)^2$, $m_3=m_4=m_t$, $m_5=m_6=m_b$ and

$$\begin{aligned} \rho_i &= \frac{\lambda^{1/2}(s_{ij},m_i^2,m_j^2)}{s_{ij}+m_i^2-m_j^2}, \\ \sigma_i &= \frac{1-\rho_i}{1+\rho_i}. \end{aligned} \tag{3.4}$$

Our calculation shows in the total cross section the soft IR singularity induced by the one-loop virtual gluon correction is exactly cancelled by the IR singularity part offered by the soft gluon emission process $\gamma\gamma \to t\bar{t}b\bar{b}$ (g). The hard gluon emission cross section σ_{hard} for $E_7 > \delta_s\sqrt{s}/2$ is finite and can be calculated numerically in four dimensions by using Monte Carlo method.

The integrations of 4-body phase space in evaluations of σ_{tree}, $\sigma_{virtual}$ and σ_{soft} are carried out by using our created 4-body phase space integration program as described in last section. But in evaluation of σ_{hard} of $\gamma\gamma \to t\bar{t}b\bar{b}$ $+g$ process, we apply CompHEP-4.4p3 program[29] to calculate the tree-level amplitude and the integration of 5-body phase space. Finally, the NLO QCD corrected total cross sections for process $\gamma\gamma \to t\bar{t}b\bar{b}$ can be obtained as

$$\sigma_{NLO} = \sigma_{tree} + \sigma_{virtual} + \sigma_{soft} + \sigma_{hard}. \tag{3.5}$$

The QCD NLO corrected cross section σ_{NLO} is both UV- and IR-finite. All the UV and IR divergences are cancelled analytically.

IV. Numerical Results and Discussions

In our numerical calculation we take following input parameters[27, 28]:

$$\begin{array}{ll} m_W = 80.403\ GeV, & m_Z = 91.1876\ GeV, \\ m_t = 172.5\ GeV, & m_b = 4.7\ GeV. \\ \alpha_{ew}(0)^{-1} = 137.0359991, & \alpha_s(m_Z^2) = 0.1176, \end{array} \tag{4.1}$$

The QCD renormalization scale μ is taken to be $\mu = \mu_0 (\equiv m_t + m_b)$ if there is no other statement, and the running strong coupling $\alpha_s(\mu^2)$ is evaluated at the three-loop level ($\overline{MS}$ scheme) with the five active flavors[27]. For the numerical calculations of one-loop integrals, we use LoopTools2.1[19] package to deal with 2-, 3- and 4-point integrals. The implementations of the scalar and tensor 5-point integrals are done exactly by using our Fortran programs as used in previous works[30, 31] with the approach presented in Ref.[32]. And the 6-point scalar and tensor integrals are evaluated by using our created programs with the expressions given in Refs.[14] and [15]. In Ref.[16], T. Binoth, et al., derived an analytic expression for the scalar hexagon function, which is convenient for the subsequent numerical integration. We checked also the numerical results of 6-point scalar integrals by using two methods presented in Refs.[14, 15] and [16], and confirmed the correctness of our 6-point scalar integral program. For example, with the Set(I) input parameters in Ref.[16] we get exactly the same numerical results as $(1.3526 \times 10^{-2} + 4.0608 \times 10^{-15}\ i)$ by using both two methods.

During our numerical calculation, we have studied the independence of the total cross section involving the NLO QCD corrections of process $\gamma\gamma \to t\bar{t}b\bar{b}$ on the soft cutoff $\delta_s (= 2\ \Delta E_7/\sqrt{s})$. To show that independence, we depict the cross section parts $\sigma_4 (= \sigma_{tree} + \sigma_{soft} + \sigma_{virtual})$, $\sigma_5 (=$

σ_{hard}) and NLO QCD corrected cross section σ_{NLO} versus δ_s in Figs.3(a-b) with $\sqrt{s} = 800$ GeV. As shown in these two figures, both σ_4 and σ_5 obviously depend on the soft cutoff δ_s, but σ_{NLO} is independent of the soft cutoff value with the best fit average value being 7.978 fb and the errors being less than 1.3% and 0.5% in the δ_s regions of $[10^{-5},\ 10^{-4}]$ and $[10^{-4},\ 5\times 10^{-2}]$, respectively. In further numerical calculation we fix $\delta_s = 10^{-3}$.

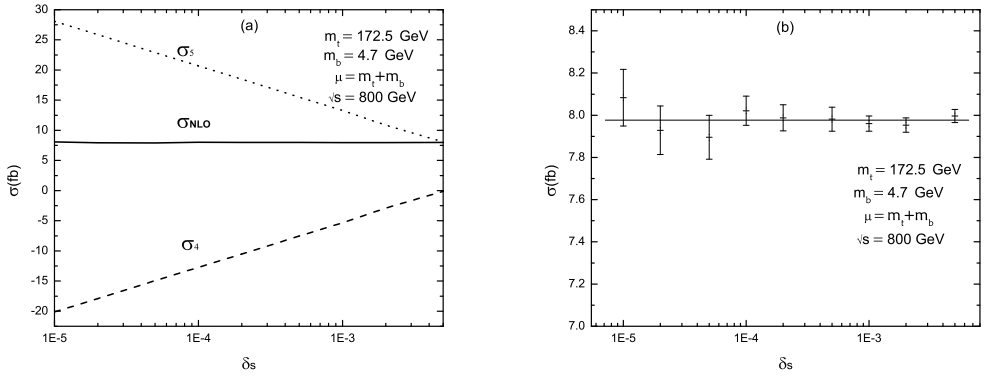

Figure 3: (a) The cross section parts $\sigma_4(=\sigma_{tree}+\sigma_{soft}+\sigma_{virtual})$, $\sigma_5(=\sigma_{hard})$ and the NLO QCD corrected cross section(σ_{NLO}) of the $\gamma\gamma \to t\bar{t}b\bar{b}$ process as the functions of the soft cutoff $\delta_s(=2\ \Delta E_7/\sqrt{s})$ with $\mu = \mu_0 = m_t + m_b$ and $\sqrt{s} = 800$ GeV. (b) The enlarged plot of Fig.3(a) for the NLO QCD corrected cross section(σ_{NLO}) with integration error versus δ_s.

We define the K-factor as the ratio of the NLO QCD corrected cross section and the LO cross section($K \equiv \frac{\sigma_{NLO}}{\sigma_{LO}}$). The numerical results of the cross section and the K-factor for the process $\gamma\gamma \to t\bar{t}b\bar{b}$ are plotted in Fig.4(a) and Fig.4(b) respectively, with the $\gamma\gamma$ colliding energy $\sqrt{s}$ running from 400 GeV to 2 TeV. In Fig.4(a), the full and the dashed curves correspond to the LO and NLO QCD corrected cross sections separately. As indicated in Fig.4(a), the cross section increases quickly as the $\gamma\gamma$ colliding energy running from 400 GeV to 2 TeV, and the NLO QCD correction obviously enhances the tree-level cross section in the plotted range of $\sqrt{s}$. The NLO QCD corrected cross section of process $\gamma\gamma \to t\bar{t}b\bar{b}$ with $\sqrt{s} = 2\ TeV$ can reach the value of 15.39 fb. Fig.4(b) shows the corresponding K-factor varies from 1.70 to 1.14 as the c.m.s energy $\sqrt{s}$ running from 400 GeV to 2 TeV. The analysis of the contribution parts of NLO QCD correction shows that in the small energy region the K-factor is enhanced due to a Coulomb singularity effect on the contribution from the diagrams with virtual gluon exchange between heavy quarks. The cross sections, σ_{tree} and σ_{NLO}, and K-factors at some typical $\sqrt{s}$

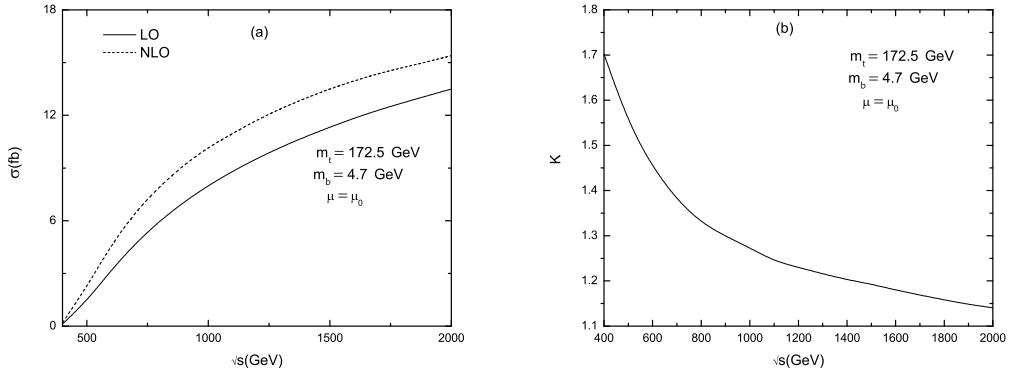

Figure 4: (a) The LO and NLO QCD corrected cross sections for the process $\gamma\gamma \to t\bar{t}b\bar{b}$ as the functions of c.m.s. colliding energy($\sqrt{s}$), (b) the corresponding K-factor versus $\sqrt{s}$.

$\sqrt{s}(GeV)$	$\sigma_{tree}(fb)$(GRACE)	$\sigma_{tree}(fb)$	$\sigma_{NLO}(fb)$	K-factor
500	1.4453(4)	1.4458(5)	2.24(1)	1.55
800	5.991(3)	5.990(4)	7.96(4)	1.33
1000	8.001(6)	8.000(7)	10.18(6)	1.27
2000	13.51(2)	13.50(2)	15.39(9)	1.14

Table 2: The LO and NLO QCD corrected cross sections, K-factors for $\gamma\gamma \to t\bar{t}b\bar{b}$ process with $\sqrt{s} = 500\ GeV$, $800\ GeV$, $1000\ GeV$, $2000\ GeV$, respectively. The LO cross section values obtained by using GRACE2.2.0 system are listed there for comparison. The number of the Monte Carlo events is 5×10^6.

points can be read out from Figs.4(a-b) and are listed in Table 2. For the correctness check of the calculation of the LO cross section for $\gamma\gamma \to t\bar{t}b\bar{b}$ process, the results obtained by using GRACE2.2.0 system are presented there too.

The renormalization scale dependence of both the LO and NLO QCD corrected total cross sections for the process $\gamma\gamma \to t\bar{t}b\bar{b}$ with $\sqrt{s} = 800\ GeV$, is plotted in Fig.5. In this figure the scale is parameterized as μ/μ_0 ($\mu_0 \equiv m_t + m_b$) and the full-line and dashed-line correspond to the LO and the NLO QCD corrected cross sections, respectively. We can see from the figure that in the region $0.75 < \mu/\mu_0 < 4$ the NLO QCD correction obviously improves the independence of the renormalization scale μ. Therefore, we can conclude that the uncertainty of the cross section for process $\gamma\gamma \to t\bar{t}b\bar{b}$ due to the variation of renormalization scale μ, can be reduced by considering the NLO QCD corrections.

The distributions of the transverse momenta of top- and bottom-quark(p_T^t and p_T^b) with the colliding energy $\sqrt{s} = 800\ GeV$, are depicted in Fig.6(a) and Fig.6(b) separately. In Fig.6(a), we

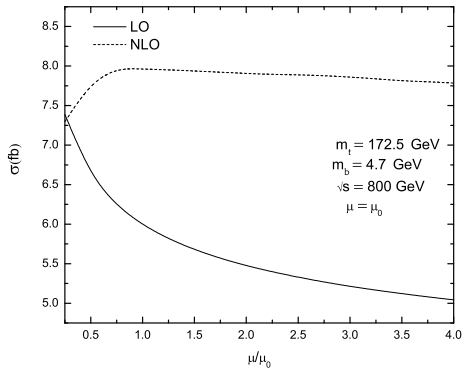

Figure 5: The LO and NLO QCD corrected cross sections for the $\gamma\gamma \to t\bar{t}b\bar{b}$ process as the functions of renormalization scale $\mu/\mu_0(\mu_0 \equiv m_t + m_b = 147.2\ GeV)$.

can see that the NLO QCD correction obviously enhances the differential cross section predicted in the SM at tree-level when the p_T^t value is less than 250 GeV. Our analysis shows that in the region 20 $GeV < p_T^t < 250\ GeV$, the large correction to the distribution of p_T^t comes mainly from the contribution of the hard gluon emission process. But when $p_T^t > 250\ GeV$, the correction to the distribution of p_T^t from the hard gluon emission process, is largely cancelled by the negative correction from virtual gluon and soft gluon emission contributions, then the p_T^t distribution corrections become to be much smaller. That means the absolute correction $(|\frac{d\sigma_{NLO}}{dp_T^t} - \frac{d\sigma_{tree}}{dp_T^t}|)$ is enhanced at low p_T^t and reduced at large p_T^t due to the momentum balance between top particles and gluons radiated from top quarks at the NLO, which reduces the momenta of the top quarks. For b-quark, we can see from Fig.6(b) that the large enhancement of the QCD corrected differential cross section$(\frac{d\sigma_{NLO}}{dp_T^b})$, which can nearly double the LO differential cross section somewhere, can be appeared in the p_T^b value range between 20 GeV and 120 GeV, while in the range of $p_T^b > 150\ GeV$ the NLO QCD correction becomes to be very small. Similar with the discussion for the distribution of p_T^t, that is also the consequence of the momentum balance between bottom particles and gluons radiated from bottom quarks at the NLO.

V. Summary

In this paper we calculate the complete one-loop QCD corrections to the process $\gamma\gamma \to t\bar{t}b\bar{b}$ at a photon-photon collider. We present the dependence of the NLO QCD correction of process

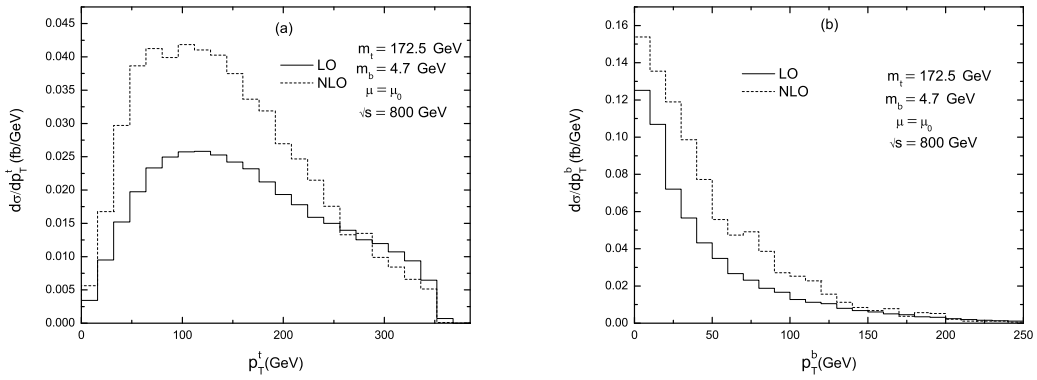

Figure 6: The distributions of the transverse momenta of top- and bottom-quark for the $\gamma\gamma \to t\bar{t}b\bar{b}$ process with $\sqrt{s} = 800\ GeV$. (a) for top-quark, (b) for bottom-quark.

$\gamma\gamma \to t\bar{t}b\bar{b}$ on colliding energy $\sqrt{s}$ in the SM, and find that NLO QCD correction can generally increase the LO cross section. It shows that in the $\gamma\gamma$ colliding energy range of $400\ GeV < \sqrt{s} < 2\ TeV$, the corresponding K-factor goes down from 1.70 to 1.14. We find that the NLO QCD correction can obviously improve the independence of the cross section for process $\gamma\gamma \to t\bar{t}b\bar{b}$ on the renormalization scale μ, and the NLO QCD correction also changes obviously the distributions of transverse momenta of the final top- and bottom-quark states.

Acknowledgments: We would like to acknowledge professor C.-S. Li for bringing our attention to this issue. This work was supported in part by the National Natural Science Foundation of China, the Education Ministry of China and a special fund sponsored by Chinese Academy of Sciences.

References

[1] Tevatron Electroweak Working Group(for the CDF and D0 Collaborations), Fermilab-TM-2347-E, TEVEWWG/top 2006/01, CDF-8162, D0-5064, hep-ex/0603039v1.

[2] I. Bigi, H. Krasemann, Z. Phys. **C7** (1981) 127; J. Kühn, Acta.-Phys.-Austr. (Suppl.) **XXIV** (1982) 203; I. Bigi, Y. Dokshitzer, V. Khoze, J. Kühn and P. Zerwas Phys. Lett. **B181** (1986) 157.

[3] C. Farrell, A. H. Hoang, Phys. Rev. **D74** (2006) 014008.

[4] V. Fadin, V. Khose and T. Sjöstrand, Z. Phys. **C48** (1990) 613.

[5] M. Strassler and M.E. Peskin, Phys. Rev. **D43** (1991) 1500.

[6] W. Kwong, Phys. Rev. **D43** (1991) 1488.

[7] Y. Sumino, K. Fujii, K. Hagiwara, H. Murayama, C.K. Ng, Phys. Rev. **D47** (1993) 56.

[8] F.J. Yndurain, Phys. Lett **B321** (1994) 400.

[9] Lali Chatterjee, Cheuk-Yin Wong, hep-ph/9501218.

[10] Han Liang, Ma Wen-Gan, Yu Zeng-hui, Phys. Rev. **D56** (1997) 265.

[11] A. Denner, S. Dittmaier, M. Strobel, Phys. Rev. **D53** (1996) 44.

[12] Chen Hui, Ma Wen-Gan, Zhang Ren-You, Zhou Pei-Jun, Hou Hong-Sheng, Sun Yan-Bin, Nucl. Phys. **B683** (2004) 196.

[13] A. Aeppli, G.J. van Oldenborgh and D. Wyler, Nucl. Phys. **B428**(1994) 126, hep-ph/9312212; W. Beenakker, F.A. Berends, A.P. Chapovsky, Nucl.Phys. **B548**(1999)3.

[14] A. Denner and S. Dittmaier, Nucl. Phys. **B734** (2006) 62.

[15] A. Denner, Fortschr. Phys. **41**(1993)**4**, 307.

[16] T. Binoth, G. Heinrich and N. Kauer, Nucl. Phys. **B654** (2003)277.

[17] A. Denner, S. Dittmaier, M. Roth, L.-H. Wieders, Phys. Lett. **B612** (2005) 223.

[18] T. Hahn, Comput. Phys. Commun. **140** (2001)418.

[19] T. Hahn, M. Perez-Victoria, Comput. Phys. Commun. **118** (1999)153.

[20] E. Byckling and K. Kajantie, 'Particle Kinematics', John Wiley and Sons, London, 1973; Stefan Weinzierl, hep-ph/0006269.

[21] J. Fujimoto, et al., Comput. Phys. Commu. 153(2003)106; T. Ishikawa, Y. Kawabata, et al., Minami-Tateya collaboration, 'GRACE User's Manual', Version 2.0.

[22] B. W. Harris and J.F. Owens, Phys. Rev. **D65** (2002) 094032, hep-ph/0102128.

[23] W. Beenakker, S. Dittmaier, M. Kramer, B. Plumper, M. Spira and P.M. Zerwas, Phys. Rev. Lett. 87 (2001) 201805; Nucl. Phys. **B653**(2003)151-203.

[24] S. Catani and M.H. Seymour, Phys. Lett. **B378** (1996) 287 and Nucl. Phys. **B485** (1997) 291 [Erratum-ibid. B **510**(1997) 291].

[25] S. Catani, S. Dittmaier, M.H. Seymour and Z. Trócsányi, Nucl. Phys. **B627** (2002) 189.

[26] L. Reina, S. Dawson and D. Wackeroth, Phys. Rev. **D65**(2002)053017; P. Wu, W.-G. Ma, R.-Y. Zhang, Y. Jiang, L. Han, and L. Guo, Phys. Rev. **D73**,(2006)015012.

[27] W.M. Yao, et al., J. of Phys. **G33**,1 (2006).

[28] F. Jegerlehner, DESY 01-029, hep-ph/0105283.

[29] E. Boos, V. Bunichev, et al., (the CompHEP collaboration), Nucl.Instrum.Meth. A534 (2004) 250-259, hep-ph/0403113.

[30] Y. You, W.-G. Ma, H. Chen, R.-Y. Zhang, Y.-B. Sun, H.-S. Hou, Phys.Lett. **B571** (2003) 85-91.

[31] R.-Y. Zhang, W.-G. Ma, H. Chen, Y.-B. Sun, H.-S. Hou, Phys.Lett. **B578**(2004) 349-358.

[32] A. Denner and S. Dittmaier, Nucl. Phys. **B658**(2003) 175.